



Stockholm  
University

# Bachelor Thesis

Degree Project in  
Geoscience 15 hp

## **Garnet-Chloritoid Micaschist as a Key to Decipher the Metamorphic Evolution of the Continental Crust: A Case Study from the Dora-Maira Massif (Western Alps)**

Mattias Barkelius



Stockholm 2022

Department of Geological Sciences  
Stockholm University  
SE-106 91 Stockholm

# Garnet-Chloritoid Micaschist as a Key to Decipher the Metamorphic Evolution of the Continental Crust: A Case Study from the Dora-Maira Massif (Western Alps)

## Abstract

The metamorphic history of a rock unit is most often described by the pressure and temperature conditions the rock experienced during metamorphism. The Alpine belt is a classical high-pressure orogen characterized by metamorphism under blueschist- and eclogite facies conditions, especially in the Western Alps. The Dora-Maira Massif is home to rocks which experienced some of the highest pressures known in the Alps, including the coesite-bearing pyrope-quartzite of the Brosasco Isasca Unit, which is a textbook example of subduction of continental crust and ultra-high-pressure metamorphism. By studying a garnet-chloritoid micaschist gathered in the Germanasca valley in the Muret Unit of the Dora-Maira Massif (red star in Fig. 1), the goal of my project is to estimate the peak pressure and temperature conditions of the Muret Unit. This was done by first, using optical microscopy to describe thin sections, which included identifying minerals, rock textures and evidence of mineral reactions. Secondly, by measuring chemical compositions using X-ray fluorescence and electron microprobe analysis. Thirdly, by calculating pressure and temperature conditions during metamorphism, using the measured chemical data and thermodynamic modelling. Peak pressure and temperature conditions were constrained by observed mineral assemblage, garnet endmember compositions and silica content of muscovite, to 510-530 °C and 22-26 kbar. These data suggest that the Muret Unit almost reached ultra-high-pressure conditions (quartz/coesite reaction at 28 kbar) and a calculated maximum burial depth of 66-78 km. Future work involving dating of metamorphic stages will allow for the calculation of exhumation rates, a requirement for the establishment of a geodynamic model explaining continental subduction and exhumation in the Muret Unit.

## Introduction

Ever since Eskola (1920) introduced the concept a century ago, metamorphic facies has been the most common way to link the minerals observed in a metamorphic rock with the pressure and temperature ( $P$ - $T$ ) conditions that the rock experienced during metamorphism. A metamorphic facies is an assemblage of minerals that recrystallized in thermodynamic equilibrium with each other. For a given chemical composition of the rock, each mineral assemblage is characteristic for a certain range of  $P$ - $T$  conditions. With the advent of experimental petrology, strong constraints have been placed on which minerals and mineral assemblages are stable at different  $P$ - $T$  conditions (Holland and Powell 2011). This has led to the metamorphic facies that are used today (Fig. 2) that describe three major types of metamorphism (Spear 1993; Liou et al. 1998). A low-pressure series of prehnite-hornfels that occurs during contact metamorphism, a medium pressure series of prehnite/pumpellyite-greenschist-amphibolite-granulite that occurs during regional metamorphism and a high-pressure series of pumpellyite-blueschist-eclogite that occurs in subduction zones.

At convergent plate boundaries, oceanic crust gets subducted under continental crust because oceanic crust has a higher density. This subjects the subducting plate to rapidly increasing pressure, while temperature increases at a slower rate, causing metamorphism at blueschist facies conditions (7-20 kbar and up to 500 °C, Fig. 2) followed by eclogite facies conditions (>13 kbar and up to 800 °C, Fig. 2) as burial depth increases. While the higher buoyancy of continental crust often keeps it from being dragged down alongside oceanic crust, subduction of continental crust does happen during major mountain building events. Some locations that record eclogite facies conditions of continental rocks are the Caledonides in Norway, the Himalayas in China and the Western Alps in Italy (Ernst and Liou 2008; Manzotti and Ballèvre in press).

The Dora-Maira Massif is part of the internal crystal massifs together with the Gran Paradiso Massif and the Monte Rosa Massif (Fig. 1). They are all remnants of the micro continent Briançonnais, which once belonged to the European paleomargin. During the main compressional event in the Eocene, the sedimentary cover was detached from the crystalline basement, resulting in different parts of the Briançonnais micro continent experiencing different grades of metamorphism (Ballèvre et al. 2020). The internal crystal massifs experienced the highest grade of metamorphism, with both the Dora-Maira and Gran Paradiso Massifs being metamorphosed at upper blueschist facies to eclogite facies conditions (Manzotti et al. 2015; Groppo et al. 2019).

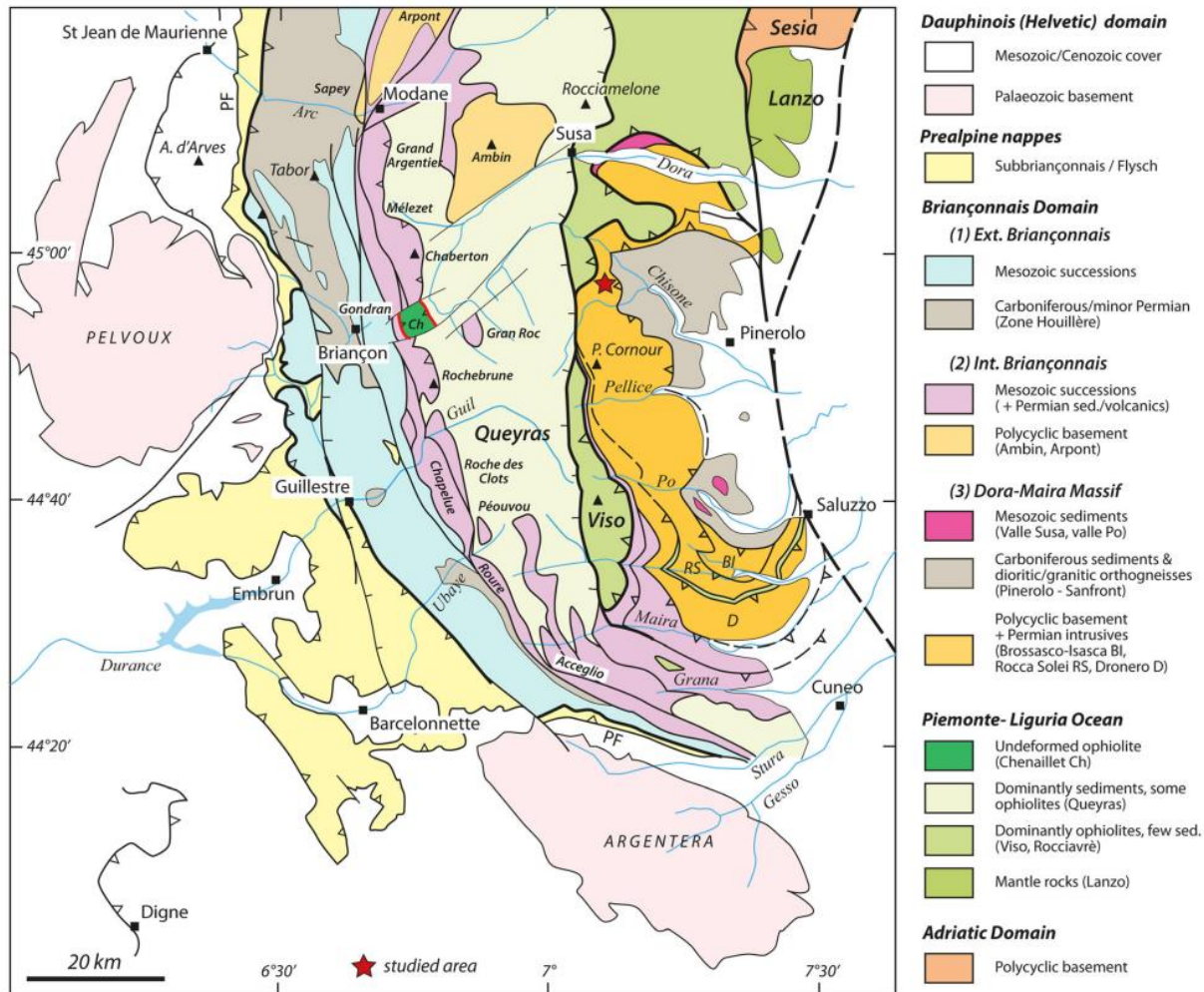


**Figure 1.** Simplified lithotectonic map of the Western Alps from Ballèvre et al. (2020). The red star marks the Germanasca Valley, where samples for both Nosenzo et al. (2021) and this study were taken.

The Dora-Maira Massif has been known for ultra-high-pressure metamorphism ever since coesite inclusions were found in garnet crystals in pyrope-quartzite rocks of the Brossasco-Isasca Unit. This discovery was early proof for ultra-high pressure metamorphism of continental crust, and showed that continental crust could be subducted to depths of over 100 km and then returned to the surface (Chopin 1984). While the ultra-high pressure unit and its neighbouring units of the southern Dora-Maira Massif are well studied at this point (Groppo et al. 2019), less is known about the northern Dora-Maira Massif. The Muret Unit in the northern Dora-Maira Massif shows evidence of two separate orogenic cycles. The Variscan orogeny at roughly 324 Ma where it experienced amphibolite facies conditions (6-7 kbar, ca 650 °C) (Nosenzo et al. 2021) and the Alpine orogeny where it experienced eclogite facies conditions (9-13 kbar, 450-550 °C) (Pognante and Sandrone 1989). The Alpine estimates were done for metabasaltic rocks, and in this study, they will be complemented by estimates for metapelitic rocks, namely a garnet-chloritoid micaschist, which is a common rock to find in high-pressure terranes (Ganguly 1969; Vuichard and Ballèvre 1988; Hoschek et al. 2010; Maldonado et al. 2016; Ghignone et al. 2021).

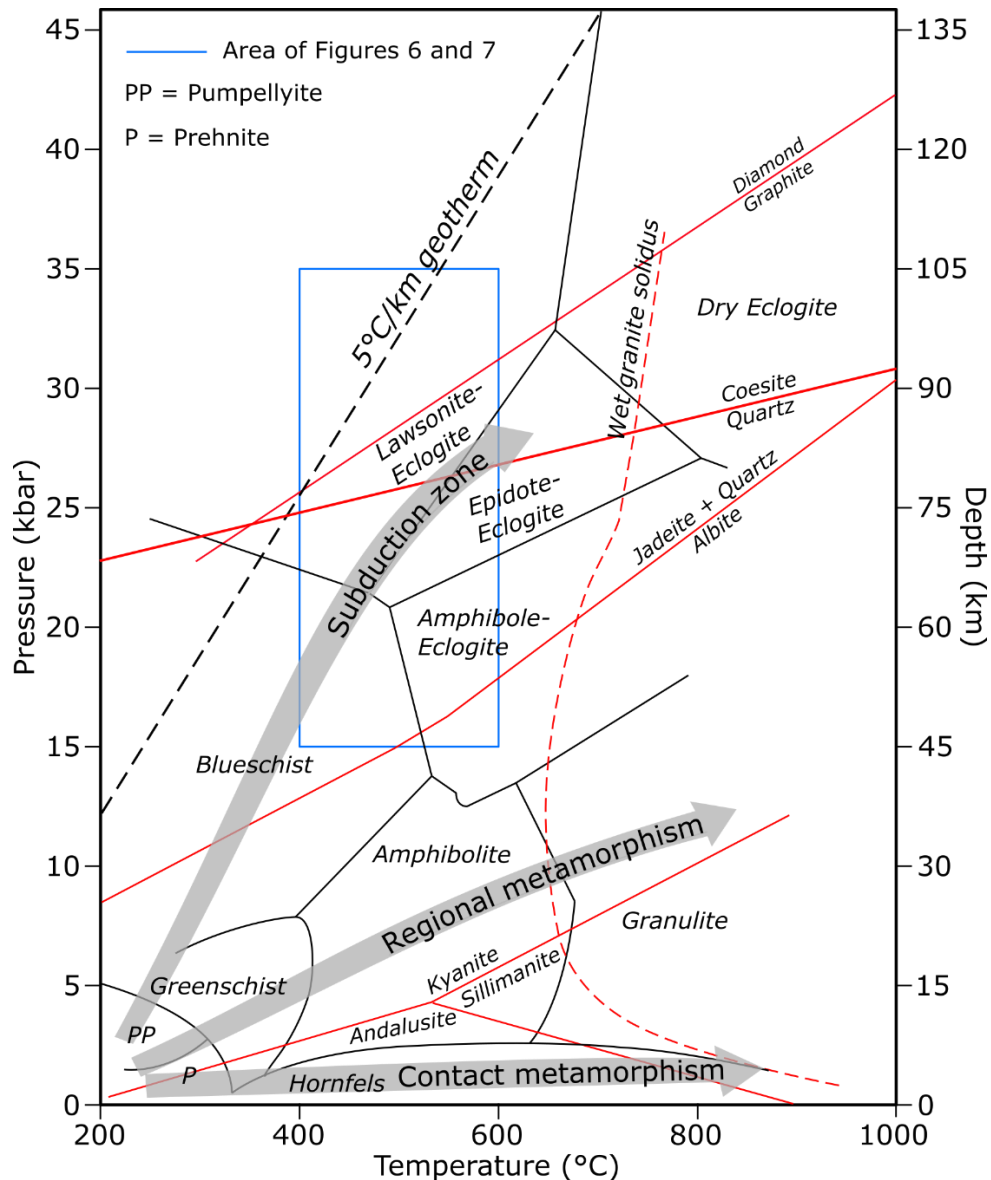


**Figure 2.** Metamorphic facies and key mineral reactions indicative of high pressure in a pressure and temperature diagram redrawn from Liou et al. (1998) and Ernst and Liou (2008). The boundary for the hornfels facies is an approximation by the author based on data in Winkler (1967). Assuming lithostatic pressure and an average continental crust density of  $3.0 \text{ kg/dm}^3$ , pressure can be converted to depth as shown (Burov et al. 2014). Black whole lines separate the different facies, red whole lines show mineral reactions, the red dashed line shows where a granite saturated with water starts to melt and the black dashed line shows the minimum temperature gradient in subduction zones, which is the lowest found in the lithosphere. The blue rectangle shows the  $P$ - $T$  range for the thermodynamic modelling in figures 6 and 7. The grey arrows show hypothetical prograde paths of three different kinds of metamorphism.  $P$  and  $PP$  in the bottom left corner stands for prehnite and pumpellyite facies respectively. The quartz/coesite reaction marks the transition into ultra-high-pressure conditions. Note that  $1 \text{ kbar} = 10^8 \text{ Pa}$ .

Many tectonic units in the Western Alps have received multiple estimates of their  $P$ - $T$  conditions over the years. While temperature estimates from different studies for any given unit generally agree with each other, there are several units where newer studies estimate higher pressures than older studies, for instance the Money unit in the Gran Paradiso Massif (Le Bayon and Ballèvre 2006; Manzotti et al. 2015) and the Pinerolo Unit in the Dora-Maira Massif (Avigad et al. 2003; Groppo et al. 2019). Since the available  $P$ - $T$  estimates for the Muret Unit were done over 30 years ago, there is reason to revisit and update those estimates with new thermodynamic modelling tools (Pognante and Sandrone 1989; De Capitani and Petrakakis 2010). As  $P$ - $T$  estimates are the first step towards building a geodynamic model of continental subduction and exhumation due to how they relate to depth (Fig. 2), it is very important to accurately determine them. Equally important is the geographic extent of different metamorphic conditions like eclogite-facies conditions, since the mechanisms for exhumation of continental crust in any model must take account for the volume of rock to be exhumed.

## Methods

Thin sections were studied under the microscope with the goal to provide a complete description of the thin sections, which was done by identifying all minerals present, estimating their relative abundance, describing the nature of any fabrics present, observing any spatial relationships between minerals, looking out for evidence of mineral reactions and relict minerals. The detailed descriptions allow for interpretation of the relative timing of minerals and structures in the rock, in turn placing constraints on the pressure-temperature calculations.

Three representative thin sections from two cut-outs (taken ca 10 cm apart) of one rock sample of a garnet-chloritoid micaschist, were studied in detail during this study. The samples were labelled GM1407A, GM1407B and GM147-b respectively, with GM1407B and GM147-b being made from the same cut-out. Microprobe measurements were made on GM147-b due to it having the most well-preserved garnets. These samples were selected carefully to find the thin sections that preserved the most information about minerals and rock textures.

The chemical composition of the rock was measured in two different ways with two different methods. First the bulk, or whole rock, chemical composition was measured using X-Ray Fluorescence (XRF) for major elements (Si, Al, Fe, Mg, Mn, Ca, Na, K, Ti, P), on samples obtained from the same rock as the thin sections were cut from. Secondly, the composition of individual mineral grains in the thin section GM147-b were measured using an electron microprobe to complement the bulk analysis. The microprobe measures the chemical composition in 1  $\mu\text{m}$  diameter sampling points on a thin section, allowing one to target individual mineral grains or parts of grains.

For one euhedral garnet crystal, the electron microprobe was used to measure the chemical composition, along a profile consisting of ca 150 sampling points. With this, variation in the amount of garnet endmembers almandine (Fe), pyrope (Mg), grossular (Ca) and spessartine (Mn) from the core to the rim was analysed. The amounts of pyrope, spessartine and grossular in the garnet core was used to inform the calculations of garnet endmember isopleths with Theriak/Domino (Fig. 7). XRF maps of the same four elements in the same garnet crystal and its surroundings, were also measured by the microprobe.

The software package Theriak/Domino was used to model equilibrium assemblages of phases (minerals and water), and to plot the resulting diagrams, in the temperature range of 400-600  $^{\circ}\text{C}$  and the pressure range of 15-35 kbar. In addition to equilibrium assemblages, Theriak/Domino was used to calculate isopleths (lines of constant composition) for three garnet end members, those being pyrope, spessartine and grossular, as well as Si atoms per formula unit (a.p.f.u.) for muscovite and the volume-percentage of the rock made up of garnet. All the calculations were done to model the conditions at the start of garnet growth in the rock, using the entire bulk composition of the rock.

The calculation, for a fixed chemical bulk composition, is based on finding the mineral assemblage with the minimal Gibbs free energy at a given point in pressure-temperature space, and then repeating the calculation across all points of the pressure-temperature space.

This produces equilibrium assemblage diagrams with temperature on the x-axis, pressure on the y-axis and various fields in the diagram. Each field represents a phase assemblage (various minerals and water) and the extent of that field represents the range of pressure-temperature conditions that assemblage is stable at (De Capitani and Brown 1987; De Capitani and Petrakakis 2010). Experimental data validates which mineral assemblage the Gibbs free energy calculation will determine to be stable (Holland and Powell 2011). Determining the pressure-temperature conditions that a sample has experienced is done by finding the field in the diagram that has the same mineral assemblage as is observed in the thin section. Further constraints are placed by comparing calculated mineral isopleths with mineral compositions measured by the microprobe, highlighting the importance of detailed thin section descriptions and well-targeted microprobe measurements.

Abbreviations used in this text are listed below (Table 1).

**Table 1.** Abbreviations of minerals and other terms used in the text. Mineral abbreviations after Holland and Powell (2011).

| <b>Mineral</b> | <b>Abbreviation</b> | <b>Other terms</b>             | <b>Abbreviation</b> |
|----------------|---------------------|--------------------------------|---------------------|
| Muscovite      | mu                  | Atoms per formula unit         | a.p.f.u.            |
| Paragonite     | pa                  | Fe/(Mg+Fe)                     | X <sub>Fe</sub>     |
| Quartz         | q                   | Na/(Na+K)                      | X <sub>Na</sub>     |
| Coesite        | coe                 | Pressure and Temperature       | <i>P-T</i>          |
| Jadeite        | jd                  | Specific foliations            | S <sub>i</sub>      |
| Glaucofane     | gl                  | Prehnite facies (in Fig. 1)    | P                   |
| Garnet         | g                   | Pumpellyite facies (in Fig. 1) | PP                  |
| Chloritoid     | ctd                 | Weight percent                 | wt%                 |
| Rutile         | ru                  |                                |                     |
| Ilmenite       | ilm                 |                                |                     |
| Chlorite       | chl                 |                                |                     |
| Lawsonite      | law                 |                                |                     |
| Carpholite     | car                 |                                |                     |
| Kyanite        | ky                  |                                |                     |
| Talc           | ta                  |                                |                     |

## Results

### *Petrographic Microscopy*

The following description is a synthesis of observations of three different thin sections (GM1407A, GM1407B and GM147-b as mentioned in the methods) of the same rock, called sample GM1407. This sample has been collected close to Fontane village, in a very vegetated area of the Germanasca valley. Since all three thin sections were cut very close to each other, they should display the same mineralogy and microstructures. The only major observed exception to this is that GM1407A did not contain any chloritoid, while the other two thin sections did, suggesting there is some compositional variation at the mesoscale.

Sample GM1407 is a garnet chloritoid micaschist dominated by quartz (30%), white mica (30%) and chloritoid (20%). Porphyroblasts up to 2 mm in size of garnet (<10%) and a completely pseudomorphed mineral (7%) occur spread evenly throughout the rock (Fig. 3). Minor amounts of rutile and ilmenite (2% together) are present as the Ti-bearing phases, with ilmenite commonly replacing rutile along grain boundaries (Fig. 3e). Chlorite and biotite are present as very rare grains in the matrix with varying orientation, though sometimes parallel to the main foliation, but are also present in partial to complete pseudomorphs of garnet and the other porphyroblast mineral.

The rock is foliated, folded and consists of bands of quartz with needle-shaped white mica alternating with bands of white mica and chloritoid. Two sets of foliations are present,  $S_1$  and  $S_2$ .  $S_1$  is defined by white mica and chloritoid oriented along isolated folds in the mica-chloritoid bands, where the hinges and part of the limbs are all that remains of the folds. The folds are isoclinal (fold limbs are parallel to each other) and the limbs are parallel with the axial plane (Fig. 3c, f, g).  $S_2$  is defined by the axial planes of the folds and is the main foliation of the rock, by product of most elongated grains being oriented parallel with it.

$S_1$  would have formed early during deformation. Later  $S_1$  was folded and transposed to  $S_2$ . Garnet crystallization was likely syndeformational with  $S_2$ , due to the larger porphyroblasts being somewhat wrapped by  $S_2$  while the smaller ones are not (Fig. 3d). Discerning the timing between garnet growth and deformation events is complicated considerably since the garnet grains in the rock, for the most part, have little to no inclusions of other minerals within them. Rutile and ilmenite are concentrated to the mica-chloritoid bands where they are oriented along  $S_1$ , but they do occur in the quartz bands as well, where they and mica needles are oriented along  $S_2$ .

Quartz displays irregular quartz-quartz grain boundaries, called interlobate boundaries, which suggest dynamic recrystallization, meaning deformation by shearing was actively happening during recrystallization (Fig. 3f). The limited recovery of quartz suggests that after deformation stopped, the  $P$ - $T$  conditions dropped too quickly to let quartz recrystallize again, statically this time. It is likely that shearing was at its most intense during folding of  $S_1$  into  $S_2$ , making it the most likely candidate for the timing of the interlobate grain boundaries.

The complete pseudomorphs of the porphyroblastic mineral that is not garnet, display a range of shapes, from anhedral to euhedral. Some grains preserve the rhombic, prismatic shape of the original mineral, a shape that is characteristic for the amphibole group (Fig. 3b). At blueschist- to eclogite-facies conditions, both amphibole and clinopyroxene are present as their Na-bearing members glaucophane and jadeite respectively, which is what they will be called for the rest of the text.

Garnet is sometimes replaced, primarily by chlorite but also by very fine-grained biotite along cracks and grain boundaries (Fig. 3a). Glaucophane on the other hand is replaced by a fine-grained mix of biotite, chlorite and likely quartz. Fine-grained biotite has also crystallized in brittle deformation structures like cracks and faults in the rock. These mineral reactions and brittle deformation happened sometime during retrograde metamorphism, on the rock's path back up to the surface.

### *Electron Microprobe measurements*

Microprobe measurements revealed that two white micas are present in the rock, muscovite and paragonite (Fig. 4). Representative measurements of garnet, chloritoid, chlorite, muscovite and paragonite are reported in Table 2.

One garnet profile of 120 points was measured with the electron microprobe, on the best-preserved garnet grain available (Fig. 3d). Chemical zoning was minimal and no sharp boundary between core and rim was found (Fig. 5). Endmember values in the core were: almandine 77-79%, grossular 6-7%, pyrope 6-7% and spessartine 9-11%. Endmember values in the rim were: almandine 80-81%, grossular 8-9%, pyrope 9-10% and spessartine 2-3%.

### *Pressure and Temperature modelling*

Constrained by the mineral assemblage, the isopleths of grossular, pyrope and spessartine, as well as the Si a.p.f.u. of muscovite, the pressure and temperature conditions for the timing of initial garnet growth are at 510-530 °C and 22-26 kbar (Figs. 6 and 7). The isopleths plot the sample in a field of garnet, chloritoid, glaucophane, jadeite and lawsonite, but only 3 of those minerals are present in the thin sections. Further inquiry with Theriak shows that jadeite and lawsonite are only present at minor to trace amounts (2-3% and <1% respectively) at those P-T conditions (510 °C and 25 kbar), meaning they could easily be removed during continued prograde metamorphism or during retrograde metamorphism.

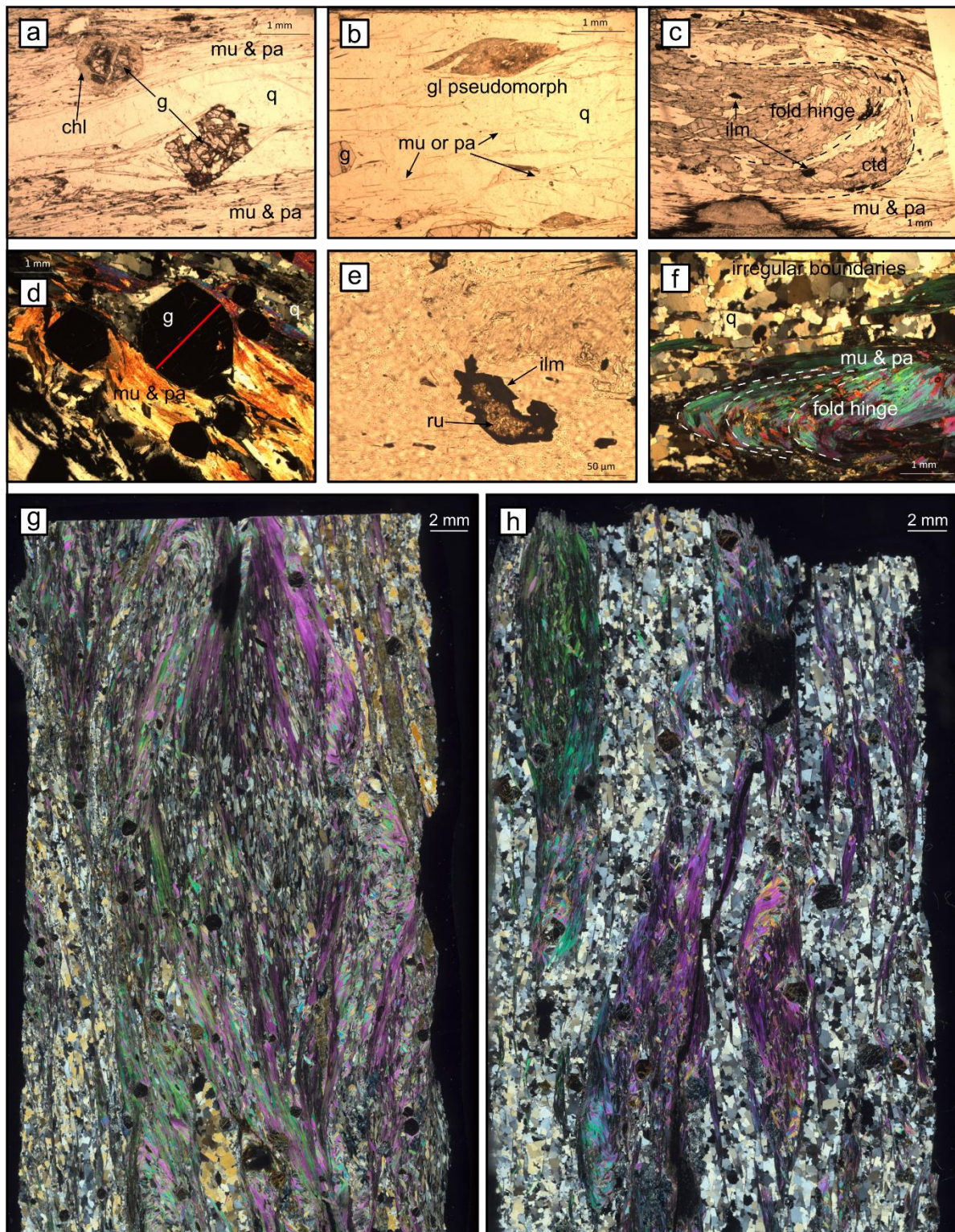


**Figure 3.** Photomicrographs of thin sections of sample GM1407, a, b, c and e are in plane polarized light while d, f, g and h are in cross polarized light. (a) Subhedral to anhedral garnet porphyroblasts replaced to a varying degree by chlorite. (b) Pseudomorphed glaucophane porphyroblast. (c) Chloritoid and white mica oriented along a fold hinge. (d) Euhedral garnet porphyroblasts with almost no inclusions. White mica wraps around the garnet. Red line shows the placement of profile measured by the microprobe in Fig. 4. (e) Rutile being replaced by ilmenite. (f) Quartz-quartz interlobate boundaries in quartz band. White mica oriented along a fold hinge in mica band. (g) Scan of thin section GM1407B, showing fold hinges defined by white mica and chloritoid. (h) Scan of thin section GM1407A showing alternating bands of quartz and white mica.

**Table 2.** Representative mineral analyses, measured by the electron microprobe. Bulk rock composition is also included, and it was measured by XRF instead. FeO in the bulk composition is calibrated from Fe<sub>2</sub>O<sub>3</sub>.  $X_{Fe} = Fe/(Fe+Mg)$  and  $X_{Na} = Na/(Na+K)$ .

| Mineral<br>Position            | Bulk   | Garnet<br>Core | Garnet<br>Rim | Chloritoid<br>Core | Chloritoid<br>Rim | Chlorite<br>Main<br>foliation | Chlorite<br>Glaucophane<br>pseudomorph | Muscovite<br>Main<br>foliation | Muscovite<br>Inclusion<br>in garnet | Paragonite<br>Main<br>foliation |
|--------------------------------|--------|----------------|---------------|--------------------|-------------------|-------------------------------|--|--------------------------------|-------------------------------------|---------------------------------|
| SiO <sub>2</sub>               | 66.26  | 36.65          | 37.20         | 24.33              | 23.76             | 25.24                         | 25.22                                  | 51.66                          | 53.14                               | 46.34                           |
| TiO <sub>2</sub>               | 0.93   | 0.05           | 0.00          | 0.03               | 0.00              | 0.06                          | 0.01                                   | 0.16                           | 0.07                                | 0.02                            |
| Cr <sub>2</sub> O <sub>3</sub> |        | 0.00           | 0.00          | 0.01               | 0.00              | 0.00                          | 0.00                                   | 0.03                           | 0.03                                | 0.01                            |
| Al <sub>2</sub> O <sub>3</sub> | 19.01  | 20.79          | 21.39         | 40.70              | 39.87             | 20.85                         | 19.95                                  | 27.44                          | 25.01                               | 41.22                           |
| FeO                            | 6.36   | 34.53          | 35.90         | 23.66              | 25.30             | 31.04                         | 26.06                                  | 2.73                           | 2.69                                | 0.83                            |
| MnO                            | 0.08   | 4.56           | 1.01          | 0.10               | 0.22              | 0.10                          | 0.07                                   | 0.00                           | 0.00                                | 0.00                            |
| NiO                            |        | 0.00           | 0.05          | 0.00               | 0.00              | 0.03                          | 0.02                                   | 0.00                           | 0.02                                | 0.00                            |
| MgO                            | 2.02   | 1.47           | 2.43          | 3.01               | 1.91              | 10.73                         | 14.16                                  | 3.32                           | 4.25                                | 0.12                            |
| CaO                            | 0.33   | 2.18           | 3.07          | 0.03               | 0.02              | 0.03                          | 0.03                                   | 0.02                           | 0.03                                | 0.06                            |
| Na <sub>2</sub> O              | 1.01   | 0.12           | 0.03          | 0.01               | 0.04              | 0.04                          | 0.09                                   | 0.20                           | 0.09                                | 7.38                            |
| K <sub>2</sub> O               | 3.91   | 0.00           | 0.00          | 0.00               | 0.01              | 0.01                          | 0.14                                   | 8.05                           | 6.41                                | 0.45                            |
| P <sub>2</sub> O <sub>5</sub>  | 0.10   | 0.00           | 0.00          | 0.00               | 0.01              | 0.01                          | 0.00                                   | 0.03                           | 0.00                                | 0.01                            |
| Total                          | 100.00 | 100.34         | 101.08        | 91.88              | 91.14             | 88.13                         | 85.76                                  | 93.64                          | 91.75                               | 96.43                           |
| Oxygen                         |        | 12             | 12            | 14                 | 14                | 14                            | 14                                     | 12                             | 12                                  | 12                              |
| Si                             |        | 2.97           | 2.97          | 2.01               | 2.00              | 2.73                          | 2.74                                   | 3.45                           | 3.58                                | 2.93                            |
| Ti                             |        | 0.00           | 0.00          | 0.00               | 0.00              | 0.01                          | 0.00                                   | 0.01                           | 0.00                                | 0.00                            |
| Al                             |        | 1.99           | 2.01          | 3.97               | 3.96              | 2.66                          | 2.55                                   | 2.16                           | 1.98                                | 3.07                            |
| Fe <sup>3+</sup>               |        | 0.08           | 0.06          | 0.00               | 0.00              | 0.00                          | 0.00                                   | 0.00                           | 0.00                                | 0.00                            |
| Fe <sup>2+</sup>               |        | 2.26           | 2.34          | 1.64               | 1.78              | 2.80                          | 2.37                                   | 0.15                           | 0.15                                | 0.04                            |
| Mn                             |        | 0.31           | 0.07          | 0.01               | 0.02              | 0.01                          | 0.01                                   | 0.00                           | 0.00                                | 0.00                            |
| Mg                             |        | 0.18           | 0.29          | 0.37               | 0.24              | 1.73                          | 2.29                                   | 0.33                           | 0.43                                | 0.01                            |
| Ca                             |        | 0.19           | 0.26          | 0.00               | 0.00              | 0.00                          | 0.00                                   | 0.00                           | 0.00                                | 0.00                            |
| Na                             |        | 0.02           | 0.00          | 0.00               | 0.01              | 0.01                          | 0.02                                   | 0.03                           | 0.01                                | 0.90                            |
| K                              |        | 0.00           | 0.00          | 0.00               | 0.00              | 0.00                          | 0.02                                   | 0.69                           | 0.55                                | 0.04                            |
| Total                          |        | 8.00           | 8.00          | 8.00               | 8.02              | 9.94                          | 10.00                                  | 6.81                           | 6.71                                | 7.00                            |
| X <sub>Fe</sub>                |        | 0.93           | 0.89          | 0.82               | 0.88              | 0.62                          | 0.51                                   |                                |                                     |                                 |
| X <sub>Na</sub>                |        |                |               |                    |                   |                               |  | 0.04                           | 0.02                                | 0.96                            |
| Almandine                      |        | 0.77           | 0.79          |                    |                   |                               |  |                                |                                     |                                 |
| Pyrope                         |        | 0.06           | 0.10          |                    |                   |                               |  |                                |                                     |                                 |
| Grossular                      |        | 0.06           | 0.09          |                    |                   |                               |  |                                |                                     |                                 |
| Spessartine                    |        | 0.11           | 0.02          |                    |                   |                               |  |                                |                                     |                                 |

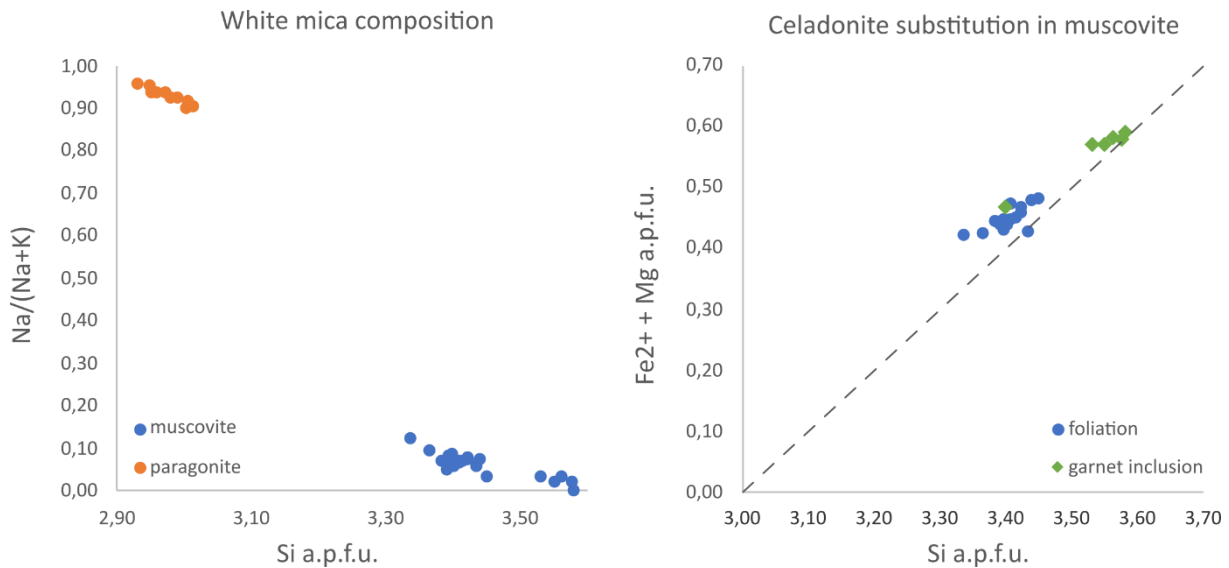


**Figure 4.** Electron microprobe measurements of white mica showing that both high Si a.p.f.u. muscovite and low Si a.p.f.u. paragonite are present in the rock. Muscovite measurements show little substitution of Fe<sup>3+</sup> and higher Si a.p.f.u. values in the grains included in garnet in Fig. 3d. The muscovite measurements suffer from poor quality due to some unknown (analytical) reason, as made evident by values of K<sub>2</sub>O wt% being lower (6-8%) than normal for muscovite (9-11%).

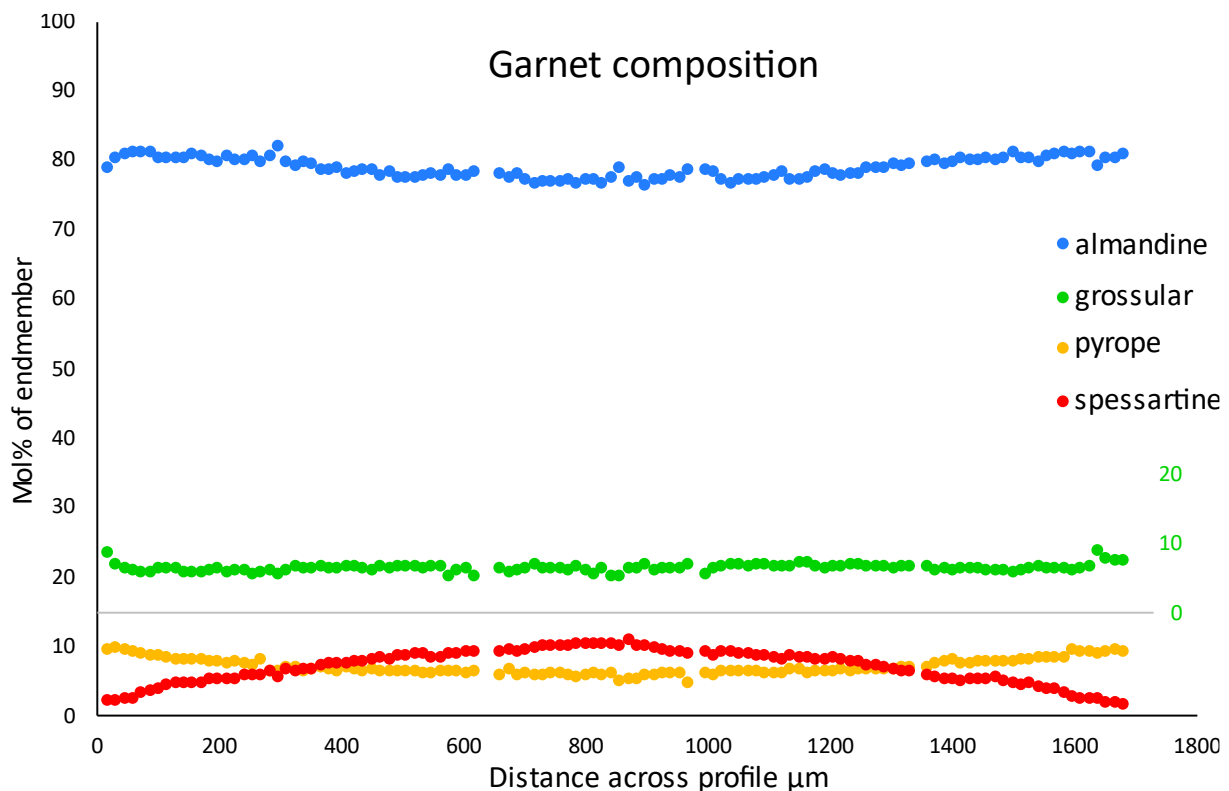


**Figure 5.** Garnet endmember composition measured by the electron microprobe across the profile shown in figure 3d. Grossular has been moved above pyrope and spessartine for the sake of visual clarity, use the y-axis on the right when viewing grossular. Slight continuous zoning can be seen in all endmembers except grossular which remains constant until the very edge of the crystal. Data gaps are due to measurements that hit inclusions of other minerals in the garnet.

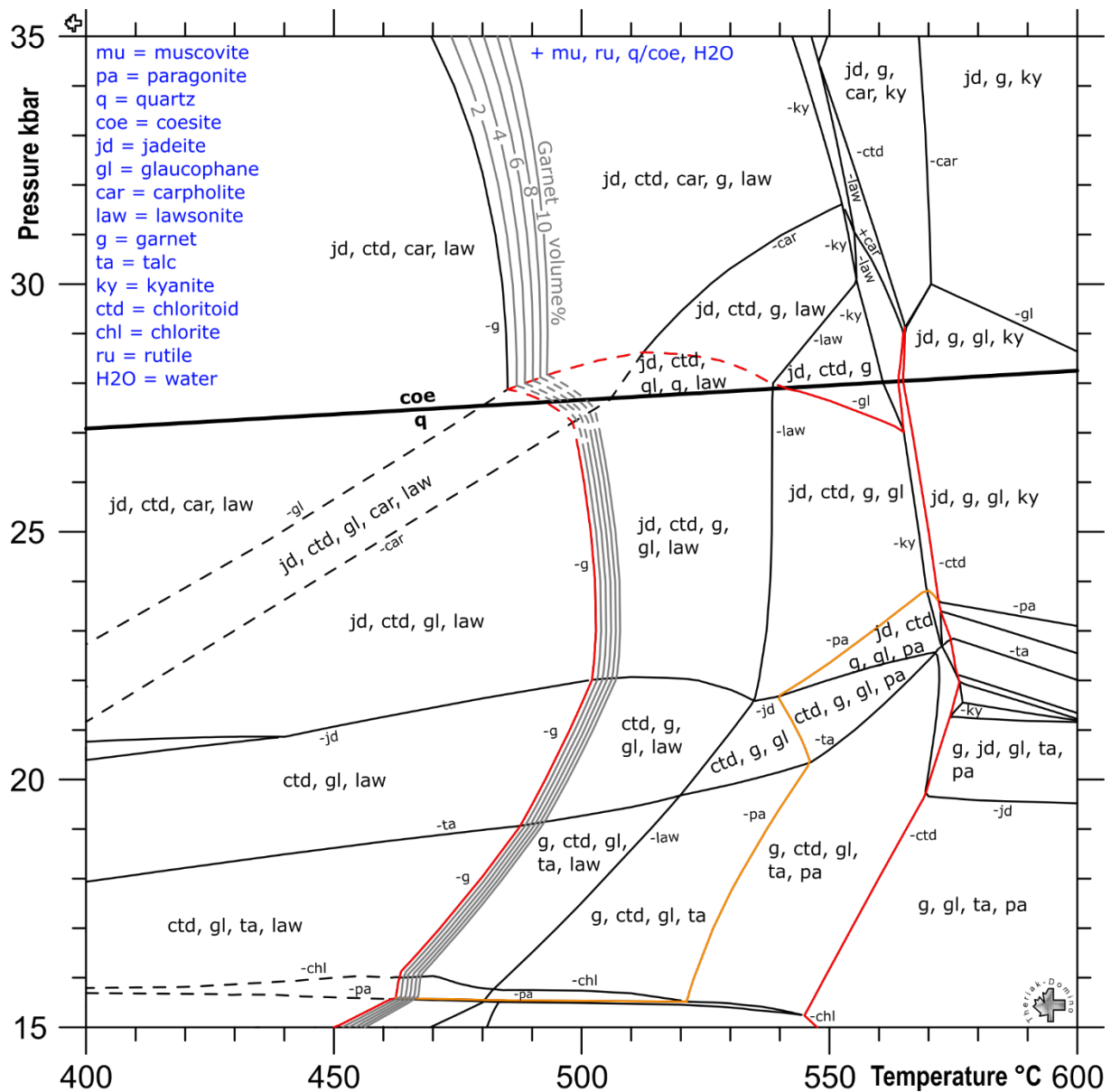


**Figure 6.** Equilibrium phase diagram, also known as pseudosection, for sample GM1407 modelled by Theriak/Domino using the database of Holland and Powell (2011). In addition to the minerals listed in each field muscovite, rutile, quartz or coesite and water were always present. Small fields are not labelled to avoid clutter. The labels with a minus-sign near the lines show on which side the mineral is unstable. The bold line showing where quartz turns into coesite marks the transition between high-pressure metamorphism below it and ultra-high-pressure metamorphism above it. The dashed lines are reactions involving glaucophane, carpholite, chlorite and paragonite that were very poorly resolved by the software, thus the dashed lines are hand drawn approximations. The amount of bulk rock volume consisting of garnet is shown by the grey lines. The red line encloses all fields where garnet, chloritoid and glaucophane coexist, the orange line encloses the fields that also have paragonite coexisting with muscovite, in addition to the previous minerals mentioned.

Glaucophane, while pseudomorphed, is still structurally present in the thin sections. Since glaucophane is still stable at 15 kbar while jadeite disappears below 21 kbar in sample GM1407, jadeite would have been altered as least as much as glaucophane, if not more, during retrogression. Since glaucophane has been altered all the way to pseudomorphs, jadeite is expected to be completely replaced by other Na-bearing phases, like albite or paragonite. The

most abundant minerals modelled at those conditions are chloritoid, muscovite and quartz, matching the abundances in the thin sections.

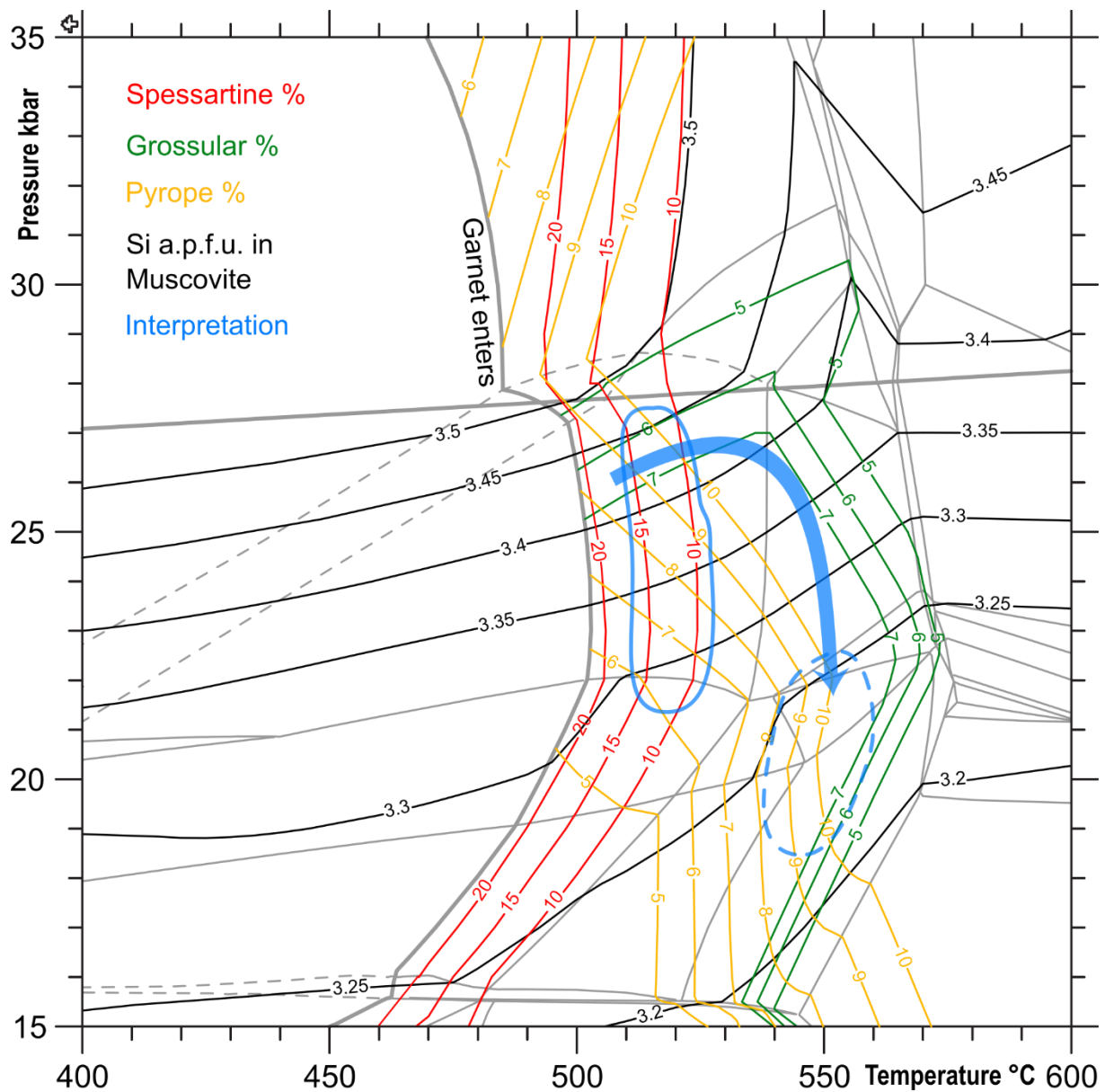


**Figure 7.** Isopleth diagram displaying the calculated molar amount of three garnet end members for values corresponding to those measured by the microprobe in sample GM1407. Also displayed are calculated isopleths for Si a.p.f.u. in muscovite and an interpretation for where in  $P$ - $T$  space garnet growth happened, the solid blue line is for the garnet core, the dashed blue line is for the garnet rim. Note that the interpretation for the garnet rim is only a prediction, for an accurate determination one would need to fractionate the composition of the garnet core from the bulk rock composition. This was not done during this study due to time constraints but would result in a slight shift of the garnet end member isopleths, as well as the stable phase assemblages. The lines from figure 6 are shown in grey for reference.

## Discussion

Eclogite-facies conditions are prevalent in the various units of the Dora-Maira Massif and *P-T* conditions are tightly constrained for the southern Dora-Maira Massif (Groppo et al. 2019). The only available *P-T* estimate for Alpine metamorphism in the northern Dora-Maira Massif is done on a metabasaltic eclogite, at a time when thermodynamic modelling of stable minerals in rocks was not as developed as it is today (Pognante and Sandrone 1989). This is likely the reason why older studies tend to give lower pressure estimates for the conditions of high-pressure metamorphism. The results from this study agree with those from previous studies on other parts of the Dora-Maira Massif (Table 3), suggesting the whole massif underwent metamorphism of similar intensity (Pognante and Sandrone 1989; Avigad et al. 2003; Groppo et al. 2019).

By assuming lithostatic pressure, any estimate of metamorphic pressure can be converted to the depth in the crust that instance of metamorphism occurred at (Burov et al. 2014). This also requires knowledge of the density of the crust, and mantle in cases of very high pressures. Due to the lack of geophysical investigations in the area, an average density of 3.0 kg/dm<sup>3</sup> is considered to be representative for the entire depth of subducted continental crust. Maximum depths reached by the different units in the Dora-Maira Massif are given in Table 3.

**Table 3.** Peak *P-T* estimates for units in the Dora-Maira Massif from the literature and this study. The estimates for the northern Dora-Maira are from Pognante and Sandrone (1989), the minimum estimates for the Pinerolo Unit are from Avigad et al. (2003) and the remaining estimates are from Groppo et al. (2019). Pressure is converted to depth by assuming lithostatic pressure and an average density of 3.0 kg/dm<sup>3</sup> (Burov et al. 2014).

| Tectonic Unit                     | Pressure Estimate<br>(kbar) | Temperature estimate<br>(°C) | Pressure converted<br>to depth (km) |
|-----------------------------------|-----------------------------|------------------------------|-------------------------------------|
| Muret (this study)                | 22-26                       | 510-530                      | 66-78                               |
| Northern Dora-Maira               | 9-13                        | 500                          | 27-39                               |
| Pinerolo (minimum estimate)       | 14-16                       | 400-550                      | 42-48                               |
| Pinerolo (maximum estimate)       | 20-23                       | 500-515                      | 60-69                               |
| San Chiaffredo                    | 21-24                       | 500-520                      | 63-72                               |
| Rocca Solei                       | 20-23                       | 510-525                      | 60-69                               |
| Dronero-Sampeyre                  | 17-18                       | 450-470                      | 51-54                               |
| Brossasco-Isasca (early prograde) | 16-23                       | 520-540                      | 48-69                               |
| Brossasco-Isasca (late prograde)  | 24-28                       | 540-560                      | 72-84                               |
| Brossasco-Isasca (peak)           | 40-43                       | 730                          | 120-129                             |

Muscovite typically has around 9-11 wt% K<sub>2</sub>O when analysed with the microprobe (Fleet et al. 2003). The muscovite crystals analysed in this study only have around 6-8 wt%, pointing to microprobe analyses of poor quality. This means that the measured Si a.p.f.u. of muscovite might not be accurate and should not be relied upon to determine the pressure at the time of initial garnet growth. The Si a.p.f.u. are made less reliable still since there are very few inclusions of muscovite in garnet. Without the textural evidence to support that muscovite equilibrated at the same time as initial garnet growth, it is impossible to rule out that muscovite did not equilibrate at an earlier or later time.

Estimating the  $P$ - $T$  conditions of growth of garnet rim, by finding the intersecting isopleths that correspond to measured end member values in the garnet rim, is the way to extend the prograde  $P$ - $T$  path. However, first one should fractionate the bulk composition of the rock by subtracting the composition of the garnet core, since those components are assumed to be locked up and unusable for the remaining garnet growth (Tinkham and Ghent 2005). This entails the calculation of a new equilibrium assemblage diagram as well as new isopleths. Most likely they would be similar to the ones using the whole bulk composition, with the most important difference being that the removal of Mn from the bulk composition shifts garnet stability, and its isopleths, towards higher temperatures (White et al. 2014). What is suggested by the current diagrams is that paragonite was not stable during the growth of garnet core, but rather became stable during growth of garnet rim. The opposite is true for jadeite, meaning it likely was replaced by paragonite during garnet growth.

Another assumption for estimating the  $P$ - $T$  conditions of garnet growth based on intersecting isopleths is that the measured end member compositions in a garnet profile remains the same during the entire duration of garnet growth. That is to say, the values for the garnet core do not change during continued growth. Enough components are used up by the garnet core to warrant fractionation of the core from the bulk composition when calculating isopleths for the garnet rim. Though estimation using the unfractionated bulk composition is still serviceable in rocks with low (< 5%) modal amounts of garnet, meaning it is applicable to the rock in this study (Zuluaga et al. 2005). However, diffusion of elements through the crystal lattice does occur, generally resulting in a smoothing of compositional profiles for garnet.

According to the thermodynamic modelling in this study, garnet should not be able to equilibrate with both 6-7% pyrope and 6-7% grossular in the core, as their isopleths do not intersect (Table 2, Fig. 7). Instead, either pyrope or grossular should have had a higher percentage in the core, suggesting that either Mg or Ca diffused out during the continued growth of the garnet crystal. Experimental data has shown that Ca is the element (out of Fe, Mg, Mn and Ca) that diffuses the slowest out of garnet at 500 °C and 20 kbar, at 2 orders of magnitude slower than Mg (Chu and Ague 2015). Additionally, the only Ca-bearing phases stable at these  $P$ - $T$  conditions are garnet and lawsonite, the latter becoming unstable later in the prograde path (Fig. 6). With nowhere to go, it is unreasonable to think that significant amounts of Ca diffused out of garnet. This makes grossular a more reliable indicator of pressure than pyrope, suggesting that the studied garnet crystallized close to the upper end of the estimated 22-26 kbar range.

The Pinerolo Unit is the structurally lowest unit in the Dora-Maira Massif and the Muret Unit is thrust on top of it.  $P$ - $T$  estimates for the Pinerolo Unit vary (Table 3), but in general, the temperature can be said to be the same as in the Muret Unit, while the pressure is lower with a difference of 0-12 kbar (Avigad et al. 2003; Groppo et al. 2019). This situation is very similar to that in the Gran Paradiso Massif, where the higher pressure Gran Paradiso Unit is thrust over the lower pressure Money Unit (Manzotti et al. 2015). Assuming that both the Pinerolo Unit and the Muret Unit reached peak  $P$ - $T$  conditions at the same time during subduction, the difference in pressure of these units can serve as a proxy for the displacement along their tectonic contact. The displacement is thus estimated at 0-36 km, with a more likely range

based on the estimate in Groppo et al. (2019) for the Pinerolo Unit, and grossular providing a better estimate than pyrope in this study for the Muret Unit, at 6-18 km. This displacement is larger than the corresponding one in the Gran Paradiso Massif at 3-15 km (Manzotti et al. 2015).

Though retrograde metamorphism of sample GM1407 is limited, it would be immensely helpful to constrain the  $P$ - $T$  conditions at a point on the rock's path back to the surface, as preparation for the next step in studying sample GM1407. That step is dating the different stages of metamorphism to provide further constraints on the kinematics of subduction, and more importantly exhumation, of continental crust. Calculated exhumation rates of high-pressure and ultra-high-pressure rocks in the Alps are on the order of a few mm to cm per year (Rubatto and Hermann 2001; Manzotti et al. 2015). These are higher than what can be explained by erosion alone, and currently favoured models all include positive buoyancy of the continental crust and tectonic forces squeezing the high-pressure and ultra-high-pressure rocks back to the surface as the main mechanisms for exhumation, though the exact details differ (Malusà and Vezzoli 2006; Malusà et al. 2011; Burov et al. 2014). This illustrates the need for  $P$ - $T$  data in more units and rock types in the Alps, to anchor conceptual and numerical models alike in the rock record.

## Conclusions

Sample GM1407 from the Muret Unit in the northern Dora-Maira Massif, is a garnet-chloritoid micaschist dominated by quartz, chloritoid, muscovite and paragonite with porphyroblasts of garnet and glaucophane pseudomorphs. Thermodynamic modelling with Theriak/Domino constrains the  $P$ - $T$  conditions to 510-530 °C and 22-26 kbar, placing it in eclogite facies conditions right below the boundary to ultra-high-pressure metamorphism, marked by the quartz/coesite transition. These results are very similar to previous estimates for eclogite facies rocks of the southern Dora-Maira Massif (e.g. Rocca-Solei Unit) and updates the estimates for the northern Dora-Maira Massif, where previous pressure estimates were considerably lower at 9-13 kbar.

## Acknowledgements

I would first and foremost like to thank my supervisor Paola Manzotti for her expertise, enthusiasm and unending support throughout the entire project. She was there to guide me every step of the way and showed me the way forward every time I got stuck. I want to thank Francesco Nosenzo and William Westin for taking their time to have many fruitful lessons and discussions on topics regarding thin sections. I also want to thank Peter Jansson for giving constructive criticism on the manuscript, which greatly improved it. Lastly, I would like to thank Helena Grönstedt for her equal parts useful and hard-to-swallow lessons on the scientific process.

## References

- Avigad D, Chopin C, Le Bayon R. 2003. Thrusting and Extension in the Southern Dora-Maira Ultra-High-Pressure Massif (Western Alps): View from Below the Coesite-Bearing Unit. *The Journal of Geology*. 111(1):57–70. doi:10.1086/344664.
- Ballèvre M, Camonin A, Manzotti P, Poujol M. 2020. A step towards unraveling the paleogeographic attribution of pre-Mesozoic basement complexes in the Western Alps based on U–Pb geochronology of Permian magmatism. *Swiss Journal of Geosciences*. 113(1):12. doi:10.1186/s00015-020-00367-1.
- Burov E, Francois T, Agard P, Le Pourhiet L, Meyer B, Tirel C, Lebedev S, Yamato P, Brun J-P. 2014. Rheological and geodynamic controls on the mechanisms of subduction and HP/UHP exhumation of crustal rocks during continental collision: Insights from numerical models. *Tectonophysics*. 631:212–250. doi:10.1016/j.tecto.2014.04.033.

Chopin C. 1984. Coesite and pure pyrope in high-grade blueschists of the Western Alps: a first record and some consequences. *Contributions to Mineralogy and Petrology*. 86(2):107–118. doi:10.1007/BF00381838.

Chu X, Ague JJ. 2015. Analysis of experimental data on divalent cation diffusion kinetics in aluminosilicate garnets with application to timescales of peak Barrovian metamorphism, Scotland. *Contrib Mineral Petrol*. 170(2):25. doi:10.1007/s00410-015-1175-y.

De Capitani C, Brown TH. 1987. The computation of chemical equilibrium in complex systems containing non-ideal solutions. *Geochimica et Cosmochimica Acta*. 51(10):2639–2652. doi:10.1016/0016-7037(87)90145-1.

De Capitani C, Petrakakis K. 2010. The computation of equilibrium assemblage diagrams with Theriak/Domino software. *American Mineralogist*. 95(7):1006–1016. doi:10.2138/am.2010.3354.

Ernst WG, Liou JG. 2008. High- and ultrahigh-pressure metamorphism: Past results and future prospects. *American Mineralogist*. 93(11–12):1771–1786. doi:10.2138/am.2008.2940.

Eskola P. 1920. The Mineral Facies of Rocks. *Norsk Geologisk Tidsskrift / Norwegian Journal of Geology*. 6:143–194.

Fleet ME, Deer WA, Howie RA, Zussman J. 2003. *Rock-Forming Minerals Volume 3A Sheet silicates: Micas*. 2nd ed. London: The Geological Society (Rock-Forming Minerals).

Ganguly J. 1969. Chloritoid stability and related paragenesis ; theory, experiments, and applications. *American Journal of Science*. 267(8):910–944. doi:10.2475/ajs.267.8.910.

Ghignone S, Borghi A, Balestro G, Castelli D, Gattiglio M, Groppo C. 2021. HP tectono-metamorphic evolution of the Internal Piedmont Zone in Susa Valley (Western Alps): New petrologic insight from garnet+chloritoid-bearing micaschists and Fe–Ti metagabbro. *Journal of Metamorphic Geology*. 39(4):391–416. doi:10.1111/jmg.12574.

Groppo C, Ferrando S, Gilio M, Botta S, Nosenzo F, Balestro G, Festa A, Rolfo F. 2019. What's in the sandwich? New P–T constraints for the (U)HP nappe stack of southern Dora-Maira Massif (Western Alps). *European Journal of Mineralogy*.:665–683. doi:10.1127/ejm/2019/0031-2860.

Holland TJB, Powell R. 2011. An improved and extended internally consistent thermodynamic dataset for phases of petrological interest, involving a new equation of state for solids. *Journal of Metamorphic Geology*. 29(3):333–383. doi:10.1111/j.1525-1314.2010.00923.x.

Hoschek G, Konzett J, Tessadri R. 2010. Phase equilibria in quartzitic garnet-kyanite-chloritoid micaschist from the Eclogite Zone, Tauern Window, Eastern Alps. *European Journal of Mineralogy*.:721–732. doi:10.1127/0935-1221/2010/0022-2049.

Le Bayon B, Ballèvre M. 2006. Deformation history of a subducted continental crust (Gran Paradiso, Western Alps): continuing crustal shortening during exhumation. *Journal of Structural Geology*. 28(5):793–815. doi:10.1016/j.jsg.2006.02.009.

Liou JG, Zhang RY, Ernst WG, Rumble D, Maruyama S. 1998. High pressure minerals from deeply subducted metamorphic rocks. In: *Ultrahigh-Pressure Mineralogy: Physics and Chemistry of the Earth's Deep Interior*. Chantilly, Virginia: Mineralogical Society of America.

Maldonado R, Ortega-Gutiérrez F, Hernández-Uribe D. 2016. Garnet–chloritoid–paragonite metapelite from the Chuac us Complex (Central Guatemala): new evidence for continental subduction in the North America–Caribbean plate boundary. *European Journal of Mineralogy*.:1169–1186. doi:10.1127/ejm/2016/0028-2578.

Malusà MG, Faccenna C, Garzanti E, Polino R. 2011. Divergence in subduction zones and exhumation of high pressure rocks (Eocene Western Alps). *Earth and Planetary Science Letters*. 310(1–2):21–32. doi:10.1016/j.epsl.2011.08.002.

Malusà MG, Vezzoli G. 2006. Interplay between erosion and tectonics in the Western Alps. *Terra Nova*. 18(2):104–108. doi:10.1111/j.1365-3121.2006.00669.x.

Manzotti P, Ballèvre M. in press. Continental subduction in the Alps: from field data to kinematic models. In: *Geodynamics of the Alps*. ISTE Ltd.

Manzotti P, Pitra P, Langlade J, Ballèvre M. 2015. Constraining P–T conditions during thrusting of a higher pressure unit over a lower pressure one (Gran Paradiso, Western Alps). *Journal of Metamorphic Geology*. 33(9):981–1002. doi:10.1111/jmg.12156.

Nosenzo F, Manzotti P, Poujol M, Ballèvre M, Langlade J. 2021. A window into an older orogenic cycle: P–T conditions and timing of the pre-Alpine history of the Dora-Maira Massif (Western Alps). *Journal of Metamorphic Geology*. n/a(n/a). doi:10.1111/jmg.12646.

Pognante U, Sandrone R. 1989. Eclogites in the Northern Dora-Maira Nappe (Western Alps, Italy): Les écloğites dans la nappe Dora-Maira septentrionale (Alpes Occidentales, Italie). *Mineralogy and Petrology*. 40(1):57–71. doi:10.1007/bf01162469.

Rubatto D, Hermann J. 2001. Exhumation as fast as subduction? *Geol*. 29(1):3. doi:10.1130/0091-7613(2001)029<0003:EAFAS>2.0.CO;2.

Spear FS. 1993. Metamorphic Phase Equilibria and Pressure-Temperature-Time Paths. *Mineralogical Magazine*. 60(403):992–993. doi:10.1180/minmag.1996.060.403.17.

Tinkham D k., Ghent E d. 2005. Estimating P-T conditions of garnet growth with isochemical phase-diagram sections and the problem of effective bulk-composition. *Canadian Mineralogist*. 43(1):35–50. doi:10.2113/gscanmin.43.1.35.

Vuichard J p., Ballèvre M. 1988. Garnet–chloritoid equilibria in eclogitic pelitic rocks from the Sesia zone (Western Alps): their bearing on phase relations in high pressure metapelites. *Journal of Metamorphic Geology*. 6(2):135–157. doi:10.1111/j.1525-1314.1988.tb00413.x.

White RW, Powell R, Johnson TE. 2014. The effect of Mn on mineral stability in metapelites revisited: new a–x relations for manganese-bearing minerals. *Journal of Metamorphic Geology*. 32(8):809–828. doi:10.1111/jmg.12095.

Winkler HGF. 1967. Hornfels Facies of Contact Metamorphism. In: *Petrogenesis of Metamorphic Rocks*. Berlin, Heidelberg: Springer. p. 64–83. [https://doi.org/10.1007/978-3-662-00866-9\\_6](https://doi.org/10.1007/978-3-662-00866-9_6).

Zuluaga CA, Stowell HH, Tinkham DK. 2005. The effect of zoned garnet on metapelite pseudosection topology and calculated metamorphic P-T paths. *American Mineralogist*. 90(10):1619–1628. doi:10.2138/am.2005.1741.